Unveiling MIMO Potential: A Prototype for Enhanced Tactical Communications with Interference Suppression

Kin-Ping Hui*, Damien Phillips*, Asanka Kekirigoda* and Alan Allwright*
J. Andrew Zhang†, Hao Zhang†, Anh Tuyen Le†, Beeshanga A. Jayawickrama†,
*Defence Science and Technology Group (DSTG), Edinburgh, Australia
†Global Big Data Technologies Centre, University of Technology Sydney, Sydney, Australia
E-mails: { Andrew.Zhang; Hao.Zhang; AnhTuyen.Le; Beeshanga.Jayawickrama;}@uts.edu.au
{Kin-Ping.Hui; Damien.Phillips; Asanka.Kekirigoda; Alan.Allwright}@defence.gov.au;

***Abstract*—This paper examines the implementation of multi-user massive MIMO technologies within wireless tactical ad-hoc networks in contested environments. By developing a real-time 8-antenna MIMO-OFDM prototype that supports SDMA communications under multiple jamming signals, we introduce innovative algorithmic solutions for interference mitigation and enhanced SDMA capabilities. These include a novel frame structure for reliable synchronization in multipath conditions and an adaptive MMSE interference suppression equalizer/receiver suitable for firmware implementation. Our findings, validated through field trials, demonstrate significant improvements in jamming suppression, offering a robust framework for secure and efficient tactical communications.**

I. Introduction

In the contemporary landscape of military operations, the evolution towards spectrum warfare necessitates a paradigm shift in the resilience of communication systems, particularly in contested environments. The crux of operational success now hinges on the reliability of tactical network infrastructures, with wireless networks being most vulnerable to disruptions, notably from radio frequency (RF) interference or jammers. Addressing these vulnerabilities call for innovative approaches to sustain communication links in such contested environments, highlighting the necessity for advancements in tactical communication strategies.

To achieve robust communications against such threats, multiple-input-multiple-output (MIMO) antenna technologies has been identified as a superior solution over traditional single antenna techniques. These advancements leverage the spatial diversity offered by employing multiple antennas, allowing for an enhanced separation of both communication and interference signals. Studies have consistently demonstrated that MIMO technologies not only facilitate a reduction in the error rates of these tactical links when faced with RF interference, but also provide a framework for more secure and efficient communications [1].

In [2], an efficient anti-jamming scheme that exploits MIMO interference cancellation and transmit precoding technologies is proposed for a 2×2 MIMO system. The method exploits the specific signal structure of 2×2 MIMO and cannot be directly extended to more general MIMO systems. In [3], a minimum mean square error (MMSE) interference suppression equalizer is proposed for MIMO-orthogonal frequency division multiplexing (OFDM) systems. Jamming signals can be effectively suppressed if they have low correlation with user signals. The work is extended to vehicular communications in [4], complying with the IEEE 802.11p standard. In [5], [6], jamming suppression is studied via exploiting the unprecedented ability to concentrate the RF energy of massive MIMO systems [7].

This study delves into the efficacy of employing multi-user massive MIMO within the framework of wireless tactical ad-hoc networks operating under contested environments. In particular, we developed a real-time 8-antenna MIMO-OFDM prototype, supporting spatial division multiple access (SDMA) communications in the presence of multiple jamming signals. Motivated by [3], we introduce novel algorithmic solutions to mitigate interference and enhance SDMA capabilities, adapting to the stringent complexity and latency requirements in firmware implementation. We introduce a new frame structure with the inclusion of a small silent period, enabling reliable synchronization in a rich multipath environment. We also propose a new minimum mean square error (MMSE) interference suppression equalizer/receiver, adapting to the firmware implementation requirement and allowing the application of more advanced detectors such as decision directed detector. These techniques enabled us to successfully implement a real-time MIMO-OFDM system with jamming suppression capability, validated by laboratory and field trials.

The rest of this paper is organized as follows. In Section II, we provide a brief introduction to the hardware of the prototype system, the signal models and an overview of baseband processing. In Section III, two key innovative algorithms for jamming suppression are elaborated. Section IV presents field trial results. Section V concludes the paper.

II. Systems and Signal Models

We consider a tactical communication network where one node uses SDMA to communicate to multiple other nodes in the presence of high-power jammers. There are N antennas at each node. There are K receive nodes and also J jammers that continuously transmit random jamming signals.

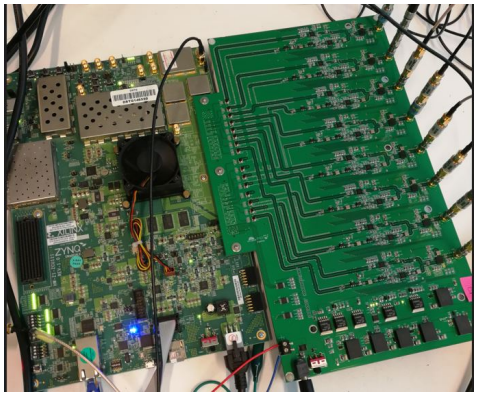

Fig. 1: The hardware transceiver consisting of ZCU111 and RF board, supporting up to 8 spatial streams.

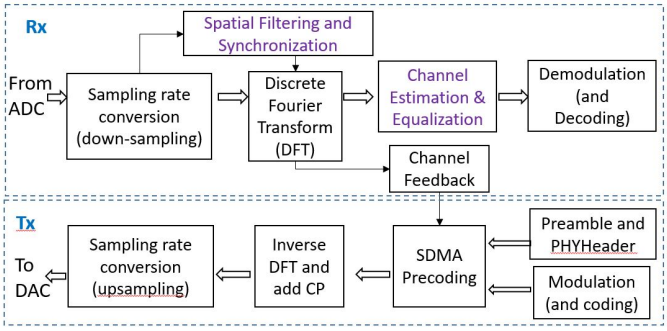

Fig. 2: Block diagram showing main baseband processing modules.

Our prototype system operates at the central frequency of 447.5 MHz, with about 5 MHz bandwidth, capable of supporting a maximum of 8 spatial streams. It uses time-division duplexing (TDD) to support uplink and downlink transmission. In the downlink, the access point (AP) uses the downlink SDMA with spatial precoding to transmit S spatial streams simultaneously to K user equipments (UEs), and each UE recovers the information by suppressing jamming signals. In the uplink, each UE uses the uplink SDMA to send information to the AP, as well as channel feedback information for precoder design at the AP. Hereafter, we will use the terms "AP" and "UE" when there is a need to distinguish them, and the term "user" to refer to a node when there is no need.

The hardware system, as shown in Fig. 1, consists of the ZCU111 board from Xilinx and customised radio front-end (RF) board, supporting 8×8 MIMO operation. The ZCU111 is a Radio Frequency System-on-Chip (RFSoC) with integrated ADCs and DACs, capable of generating and processing high-frequency signals of several GHz directly. Therefore, we adopted an efficient RF direct conversion structure, where 450 MHz signals are directly generated from and input to the ZCU111 board and the RF board only implements amplifying and filtering functions.

A. Signal Models

Considering the current signal bandwidth and future extendability, we implemented an MIMO-OFDM system. It is known that for MIMO-OFDM, the signal model at one subcarrier resemble that of a narrowband MIMO system. Therefore, for simplicity, we will drop the subcarrier index and consider the signal processing for any given subcarrier, unless noted otherwise. Due to the page limit, we only describe the processing with respect to the downlink in this paper, while the uplink is largely similar. In the downlink, the number of spatial data streams for receive node k is S_k, where $S_k \leq N$, and the total number of spatial streams is $S = \sum_{k=1}^{K} S_k$.

Let us consider a vector signal $\tilde{\mathbf{x}}_k$ of length S_k being transmitted to receiving node k, at a given subcarrier in one MIMO-OFDM symbol. Let $\mathbf{P}_k$ be the precoding matrix applied at the transmitter for receiving node k, with size of $N \times S_k$. The received signal vector of length N at the receive node k, at the corresponding subcarrier, is given by

$$\begin{aligned}\tilde{\mathbf{y}}_k &\approx \tilde{\mathbf{H}}_k\mathbf{P}_k\tilde{\mathbf{x}}_k + \tilde{\mathbf{H}}_k\sum_{i\neq k}^{K}\mathbf{P}_i\tilde{\mathbf{x}}_i + \sum_{j=1}^{J}\tilde{\mathbf{Z}}_{k,j}\tilde{\mathbf{g}}_j + \tilde{\mathbf{n}}_k,\\ &= \tilde{\mathbf{H}}(\tilde{\mathbf{x}}^T, \tilde{\mathbf{g}}_1^T, \cdots, \tilde{\mathbf{g}}_J^T)^T + \tilde{\mathbf{n}}_k, \end{aligned} \quad (1)$$

where $\tilde{\mathbf{H}} = (\tilde{\mathbf{H}}_1\mathbf{P}_1, \cdots, \tilde{\mathbf{H}}_K\mathbf{P}_K, \tilde{\mathbf{Z}}_{k,1}, \cdots, \tilde{\mathbf{Z}}_{k,J})$, $\tilde{\mathbf{x}} = (\tilde{\mathbf{x}}_1^T, \cdots, \tilde{\mathbf{x}}_K^T)^T$, $\tilde{\mathbf{H}}_k \in \mathbb{C}^{N\times N}$ denotes the channel matrix between the transmit node and receive node k; $\tilde{\mathbf{Z}}_{k,j} \in \mathbb{C}^{N_k\times 1}$ is the channel between jammer j and receive node k; $\tilde{\mathbf{x}}$ and $\tilde{\mathbf{g}}$ stand for the signals transmitted from the transmit node and jammers respectively; and $\tilde{\mathbf{n}}_k$ is the background noise which is modelled as an additive white Gaussian noise (AWGN) with independent and identically distributed (i.i.d.) entries of zero mean and variance σ^2.

Note that in (1), the approximation is due to that the received frequency-domain jamming signal is not strictly the product between transmitted signals and channels. This is because no cyclic prefix (CP) is applied to the jamming signals, and hence the linear convolution between jamming signals and the channels cannot be converted to circular convolution. Therefore, the jamming signals cannot be fully removed with the proposed method as will be elaborated later.

B. Overview of Baseband Processing

The main modules in the baseband signal processing are illustrated in Fig. 2. At the transmitter (Tx), SDMA precoding is applied subcarrier-wise to the coded and modulated signals, then the signals are converted to the time domain via inverse discrete Fourier transform (IDFT), and the baseband signal is then upsampled to match the high sampling rate set in the ZCU111 to directly generate the 450 MHz carrier frequency. The upsampled RF signal is then converted to analog by the built-in DAC on the ZCU111. At the receiver (Rx), the discrete signal is first downsampled to the baseband. A spatial filter is then generated from and applied to the received signals to suppress jamming signals, so that synchronization can be achieved. After synchronization, the signals are segmented by removing the CP, and then converted to the frequency domain via DFT. Channel estimation and equalization are then conducted, followed by demodulation and decoding.

The precoding design has been reported in our previous paper [8], and is thus omitted here. Next, we focus on describing how jamming suppression is achieved by using innovative techniques. Our techniques were motivated by the work in [3], but with significant modifications and optimizations adapted to the requirements for firmware implementation and frequency-selective jamming suppression.

III. Key Innovations in Signal Processing for Jamming Suppression

There are two major innovations in signal processing for jamming suppression: (1) time-domain spatial filtering (TDSF); and (2) frequency-domain interference suppression minimum mean square error (FD-MMSE) equalization. TDSF is mainly used to suppress some of the jamming signals such that synchronization and carrier frequency offset (CFO) estimation can be conducted. However, it cannot fully remove jamming signals, so further FD-MMSE processing is required. When spatial filters of low rank need to be used, they cannot be applied to signals for channel estimation and equalization, as the degrees-of-freedom (DoFs) of spatial streams will otherwise be reduced.

A. Synchronization with TDSF

As highlighted in [3], jamming signals can be suppressed by using the MMSE interference suppression equalizer. Therefore, the key challenge, from the signal processing viewpoint, is how to realize synchronization in the presence of jamming signals. In [3], the authors proposed to use a time-domain spatial filter obtained from the left singular vectors of the channel correlation matrix computed from received signals including both jamming and user signals. However, when the antenna number is much smaller than the DoFs of the signals, the eigenvectors will fail to sufficiently differentiate between the signal spaces between users and jammers, leading to insufficient SINR for synchronization. This happens typically when there are a number of channel paths for the users and/or jammers. To resolve this problem and achieve more reliable synchronization, we propose to use a new frame structure, where signals are prepended with a small silent period in the beginning, as shown in Fig. 3. During such period, nodes are not transmitting any signals and only the jamming signals are received. Therefore, the DoFs in the signals are only due to jamming signals and the null space of the signals can be estimated. While the underlying concept is simple, the actual implementation is still complicated as elaborated below.

The block diagram of synchronization with the assistant of TDSF is shown in Fig. 4. The TDSF is obtained by computing the null space of jamming signals during the silent period. It is then applied to the received signals, and the packet detection algorithm is applied.

1) Spatial Filter Generation: Represent the ℓ-th received time-domain signal sample at all antennas as $\mathbf{y}_\ell$ of size 8×1. The signals are first passed to a correlator, which computes the signal correlation matrix over L samples. To save computational complexity, the correlator is computed in a windowed and iterative way, that is

$$\mathbf{\Phi}_\ell = \sum_{t=\ell-L+1}^{\ell} \mathbf{y}_t \mathbf{y}_t^H = \mathbf{\Phi}_{\ell-1} + \mathbf{y}_\ell \mathbf{y}_\ell^H - \mathbf{y}_{\ell-L} \mathbf{y}_{\ell-L}^H. \quad (2)$$

Ideally, the null space can be computed by using the singular value decomposition (SVD) of the 8×8 correlation matrix $\mathbf{\Phi}_\ell$. Unfortunately, direct computation in firmware is found to be both resource and time prohibitive. The *Power Method* is a reduced-complexity iterative method for computing principal eigenvalues and eigenvectors, which essentially are the signal spaces for jammers. However, simulation results reveal that only two principal eigenvectors are feasible in terms of complexity and accuracy. In this case, the spatial filters can only fully suppress jamming signals with two equivalent propagation paths. Therefore, an alternative method is required.

Fortunately, rank-revealing QR decomposition (QRD) can generate null spaces of a matrix. In this specific type of QRD of $\mathbf{\Phi} = \mathbf{QR}$, the last several columns of the $\mathbf{Q}$ matrix, which correspond to smallest diagonal elements (right-bottom submatrix) in the $\mathbf{R}$ matrix, are the null space of $\mathbf{\Phi}$. Note there is a trade-off here between jamming suppression and the retaining of DoF of signals, when the channels between jammers and users are independent. Therefore, if we take the conjugate of the last two columns as the spatial filter for example, we can in principle fully suppress jamming signals with up to $N-2$ propagation paths, and have DoF of two for filtered user signals. The number of columns used is a design choice or a system parameter depending on applications and scenarios. In this example, we can use the filtered signals with

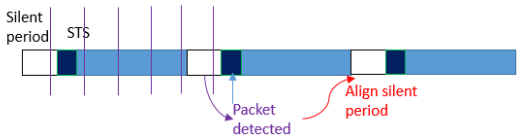

Fig. 3: Frame structure with added silent period. The silent period is generally fixed, while the receiver is designed to tolerate small variations. The purple vertical lines show the period of updating and applying the spatial filter at power on, until the packet is detected, and then the filter coefficients will be fixed over the period of one packet.

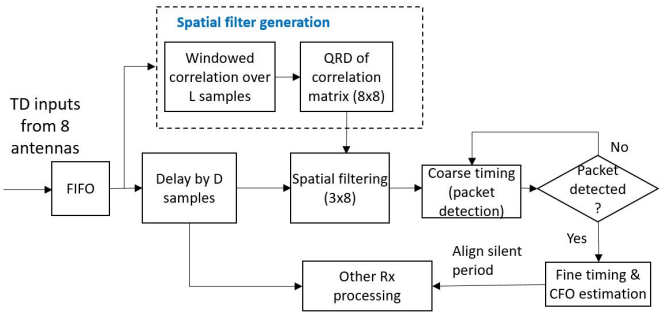

Fig. 4: Synchronization with TDSF. D is larger than the delay in spatial filter generation.

reasonably large user signal power for synchronization and CFO estimation. However, we cannot use them for channel estimation and equalization due to their low DoF. Fortunately, this is not an issue as our MMSE equalizer can independently suppress jamming signals, once synchronization and CFO estimation are completed.

2) Application of TDSF: The spatial filter generation (mainly QRD) is still time-consuming, which causes difficulties in real-time implementation. Before we know the location of the silent period, we cannot easily identify whether the correlation matrix input to the QRD corresponds to the silent period. Although the ratio between the first principal eigenvalue and the overall signal power (equal to the trace of the correlation matrix) is a good indicator for narrowband jamming channels, it becomes less accurate when frequency selectivity increases. Therefore, we need to use packet detection, which is typically based on the autocorrelation of received signals, as an indicator of alignment to the silent period.

Before knowing the approximate location of the silent period, it takes many samples from the input to the windowed correlation of TDSF to the completion of packet detection processing. Therefore, packet detection becomes "non-real-time" in the pipeline implementation. As a result, it will take a few packets to acquire the packet at power-on or out-of-sync situations, when the node does not know the approximate initial position of the silent period. Therefore, spatial filters are updated at a short interval spanning, e.g., 3.2 OFDM symbols, where the fractional number is used to ensure that $\mathbf{\Phi}$ covers different parts of signals, until the silent field is aligned and a packet is detected. After a packet is detected, filter coefficients will be fixed over a frame period and then updated in the next silent period (tracking stage). These are illustrated in Fig. 4.

To balance the initial packet acquisition time, the implementation complexity, and the spectrum efficiency, the length of the silent period needs to be carefully decided. Currently, the length of silent period is set at 96 samples, equaling to 1.5 times of an OFDM symbol period.

The effect of TDSF depends on both the frequency selectivity of the jamming channels and the similarity between the jamming channels and user channels. If the jamming channels are narrow band, TDSF can remove the majority of jamming signals; and the efficiency decreases with increasing frequency selectivity. The similarity also has a major impact on system performance: if the jamming and user channels are similar, then user signals will also be removed when applying TDSF. This is a similar issue for the FD-MMSE and probably all potential techniques for jamming suppression, as channel difference is the main property being exploited for jamming suppression.

B. FD-MMSE

FD-MMSE is applied to remove jamming signals, working independently of the TDSF. It exploits the capability of a multiple-antenna receiver in suppressing spatial interference, provided that the number of receiver antennas is larger than the total number of interferers and UE streams. The FD-MMSE is applied to each subcarrier. Suppose that N antennas are used to transmit $M < N$ independent streams. For simplicity, we drop the indexes for subcarrier and UEs here.

For a given subcarrier of a given UE, the original FD-MMSE as proposed in [3] has the form of

$$\mathbf{W}_o = \mathrm{E}[\tilde{\mathbf{x}}\tilde{\mathbf{y}}^H]\mathrm{E}[\tilde{\mathbf{y}}\tilde{\mathbf{y}}^H]^{-1}, \tag{3}$$

where $\mathrm{E}[\cdot]$ denotes the expectation operator. When the expectation is calculated from the known training signals, $\mathbf{W}_o$ can be approximated as

$$\mathbf{W}_o = \tilde{\mathbf{X}}_T\tilde{\mathbf{Y}}_T^H(\tilde{\mathbf{Y}}_T\tilde{\mathbf{Y}}_T^H)^{-1}, \tag{4}$$

where $\tilde{\mathbf{X}}_T$ is the known frequency-domain training signal matrix of size $M \times K$, with K being the number of training OFDM blocks, $\tilde{\mathbf{Y}}_T$ is the corresponding received signal matrix of size $N \times K$. For an effective FD-MMSE, $N \geq M + J$ and $K \geq M + J$ are required, where J is the number of independent jamming streams. Then the transmitted signals are estimated as

$$\hat{\tilde{\mathbf{x}}} = \mathbf{W}_o\tilde{\mathbf{y}}. \tag{5}$$

Using this method, $J \leq N - M$ independent jamming signals can be suppressed.

However, applying the above equalizer requires the algorithm to compute the inversion of a $N \times N$ matrix which has very high complexity and delay, as well as numerical stability issues in firmware implementation. It is also inconvenient to combine more advanced subsequent detectors such as decision directed detectors and sphere decoders with the equalizer. Therefore, we formulate the MMSE equalizer in another way as detailed next.

We first represent the FD-MMSE equalization matrix, $\mathbf{W}$ of size $M \times N$, in another form as

$$\mathbf{W} = \tilde{\mathbf{X}}_T(\tilde{\mathbf{Y}}_T^H\tilde{\mathbf{Y}}_T)^{-1}\tilde{\mathbf{Y}}_T^H. \tag{6}$$

When $K = N$, almost identical performance can be achieved by (6), compared to (4). Then the transmitted data symbols $\tilde{\mathbf{x}}$ at the subcarrier, including symbols for all UEs, can be estimated at the k-th UE as

$$\hat{\tilde{\mathbf{x}}} = \mathbf{W}\tilde{\mathbf{y}} = \tilde{\mathbf{X}}_T(\tilde{\mathbf{Y}}_T^H\tilde{\mathbf{Y}}_T)^{-1}\tilde{\mathbf{Y}}_T^H\tilde{\mathbf{y}}. \tag{7}$$

Directly applying the equalizer in (7) also requires the computation of matrix inversion $(\tilde{\mathbf{Y}}_T^H\tilde{\mathbf{Y}}_T)^{-1}$. Recalling that in a conventional MIMO system with signal model $\tilde{\mathbf{y}} = \tilde{\mathbf{H}}\tilde{\mathbf{x}}$, equalization involving channel inversion is typically alternatively realized via QRD or Cholesky decomposition (CLD). For positive definite matrices, CLD has much lower complexity and delay than QRD in firmware implementation. Hence, we would like to apply such CLD-based processing to the FD-MMSE. But the term $\tilde{\mathbf{X}}_T$ is not invertible. So we apply the following revision to (7) to obtain a virtually invertible matrix.

We design $\tilde{\mathbf{X}}_T$ of size $M \times K$ satisfying $\tilde{\mathbf{X}}_T\tilde{\mathbf{X}}_T^H = \mathbf{I}$. We expand $\mathbf{X}_T$ to an orthonormal matrix of $\mathbf{B}_T = (\mathbf{A}_T; \tilde{\mathbf{X}}_T)$ of size $K \times K$, where the operator ";" denotes vertical concatenation of two matrices or vectors. Since $\tilde{\mathbf{X}}_T$ are typically designed as a submatrix of an orthonormal matrix, e.g., a Hadamard matrix, $\mathbf{B}_T$ is just the full Hadamard matrix. Then

we have

$$(\hat{\boldsymbol{\alpha}}; \hat{\tilde{\mathbf{x}}}) = (\mathbf{A}_T; \tilde{\mathbf{X}}_T)(\tilde{\mathbf{Y}}_T^H \tilde{\mathbf{Y}}_T)^{-1} \tilde{\mathbf{Y}}_T^H \tilde{\mathbf{y}}, \tag{8}$$

where $\boldsymbol{\alpha}$ shall be zero in the absence of interference or corresponds to mapped interference signals otherwise, and $\hat{\boldsymbol{\alpha}}$ denotes its estimate. We can then do the following conversions:

$$\tilde{\mathbf{Y}}_T^H \tilde{\mathbf{y}} = (\tilde{\mathbf{Y}}_T^H \tilde{\mathbf{Y}}_T) \mathbf{B}_T^H (\boldsymbol{\alpha}; \tilde{\mathbf{x}}) \tag{9}$$

$$\Longrightarrow (\mathbf{B}_T \tilde{\mathbf{Y}}_T^H) \tilde{\mathbf{y}} = (\mathbf{B}_T \tilde{\mathbf{Y}}_T^H)(\mathbf{B}_T \tilde{\mathbf{Y}}_T^H)^H (\boldsymbol{\alpha}; \tilde{\mathbf{x}}). \tag{10}$$

Note that a submatrix of $(\mathbf{B}_T \tilde{\mathbf{Y}}_T^H)$ will be the channel estimate in the absence of jamming signals, but this is no longer true with jamming signals present. In general, since it can be obtained from the received training symbols, we just apply it to the received signals $\tilde{\mathbf{y}}$.

Now we can apply CLD to $(\mathbf{B}_T \tilde{\mathbf{Y}}_T^H)(\mathbf{B}_T \tilde{\mathbf{Y}}_T^H)^H$ and obtain

$$(\mathbf{B}_T \tilde{\mathbf{Y}}_T^H)(\mathbf{B}_T \tilde{\mathbf{Y}}_T^H)^H = \mathbf{L}\mathbf{L}^H, \tag{11}$$

where $\mathbf{L}$ is an upper triangular matrix. With CLD, we can readily obtain

$$(\mathbf{L}^H)^{-1} \tilde{\mathbf{y}} = \mathbf{L} \tilde{\mathbf{x}} \tag{12}$$

and then apply a decision directed detector to get the estimate $\tilde{\mathbf{x}}$. That is, starting from the bottom, one new symbol is demodulated from the equalized signal in each row and then removed from the next row. The demodulated symbols for the k-th UE are then decoded. The method can achieve much better performance by reducing inter-symbol interference, compared to conventional zero-forcing equalization.

To improve numerical stability, a regulation operation is applied to obtain $(\mathbf{B}_T \tilde{\mathbf{Y}}_T^H)(\mathbf{B}_T \tilde{\mathbf{Y}}_T^H)^H + \epsilon \mathbf{I}$ before Cholesky decomposition, where ϵ is a small value. This is because $(\mathbf{B}_T \tilde{\mathbf{Y}}_T^H)(\mathbf{B}_T \tilde{\mathbf{Y}}_T^H)^H$ is generally not a full-rank matrix and will otherwise lead to rows with very small coefficients in $\mathbf{L}$. The value of ϵ cannot be too large, as it contributes to an interfering term. In practical implementation, we have it as an adjustable parameter in firmware.

In principle, FD-MMSE can fully remove the interference. However, since the training sequence is not infinite, there is a difference between the numerical correlation and the statistical correlation, and there will still be residual errors. In addition, jamming signals do not follow the OFDM format (no cyclic prefix), and the frequency domain expression does not perfectly describe the form of received jamming signals. This contributes additional equalization errors.

IV. Field Trial Results

In the current system, each node uses a 8-element circular antenna array, as shown in Fig. 5a. The assembled unit is shown in Fig. 5b with the size of $50L \times 41W \times 13H$ in cm. The OFDM signal has 64 subcarriers, with a signal bandwidth of about 5 MHz. A CP of 16 is used.

A number of indoor and outdoor experiments were conducted and the following field trial was the most recent as we write the paper. It was carried out in an open outdoor area as shown in Fig. 6. The setup includes one AP, two UEs and one single-antenna jammer. The distance between the AP and each of the two UEs is about 50 meters. The

(a) Circular antenna array (b) Transceiver

Fig. 5: The assembled system ready for outdoor applications.

Fig. 6: Site where the field trial was conducted.

distances between the jammer and the two UEs are about 70 and 30 meters, respectively. Only downlink transmission was tested. Our real-time systems can capture 8192 continuous samples in the buffer from various sources, such as received signals, measured SNR values, and the equalized signals. Our presentation of results next are based on such captured datasets.

During the test, UE1's operation was found to be hardly affected by the jamming signals due to their large separation. So the testing results here are mainly reported for UE2. Also, in such a testing environment, the spatial channels demonstrate limited degree of freedoms. This is evidenced from Fig. 7, which shows one selected testing result for the measured SNR of four spatial data streams at the receiver in the absence of jamming signals. The SNR is computed as the reciprocal of the error vector magnitude, the power of difference between the equalized signals and the demodulated symbols. In the following results, we refer to the stream with the best performance.

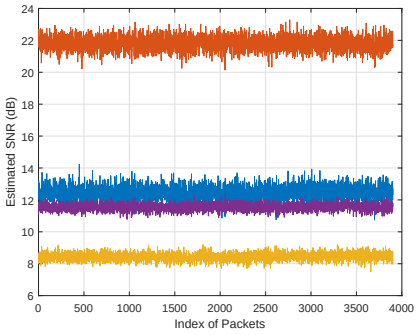

Fig. 7: Measured SNR of four spatial streams in the absence of jamming signals.

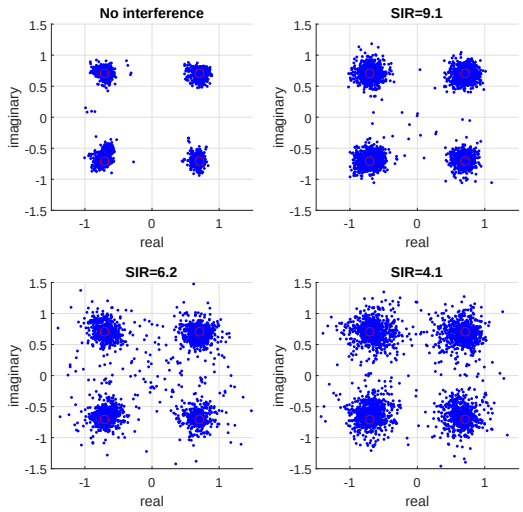

Fig. 8: Constellation plot of the equalized signals with different power levels of jamming signals. SIR values are in dB.

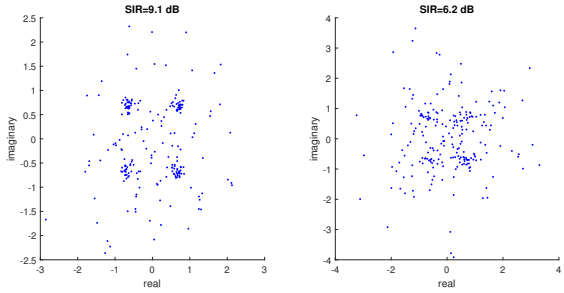

Fig. 9: Constellation plot of the equalized signals using conventional zero-forcing equalization without interference suppression.

Fig. 8 shows the constellation plots of the equalized signals for 32 packets in four cases: without jamming signals and with 3 different signal-to-jamming power ratios (SIR). The SIR is measured from the received AP signals and jamming signals. For comparison, the constellation plots for the case using conventional zero-forcing equalization are shown in Fig. 9, where the equalization is applied to three captured received signal packets in Matlab. Comparing Fig. 8 with Fig. 9, we can clearly see the improvements achieved by the proposed interference suppression scheme.

The measured SNR results for the four scenarios are accordingly illustrated in Fig. 10. In average, about 8 dB improvement is achieved for each of the jamming power levels by our scheme.

V. Conclusions

Our study demonstrates the significant potential of multi-user massive MIMO technologies to enhance the resilience and efficiency of wireless tactical ad-hoc networks in contested environments. Through the development and implementation of a real-time MIMO-OFDM prototype equipped with advanced interference mitigation and SDMA capabilities, we

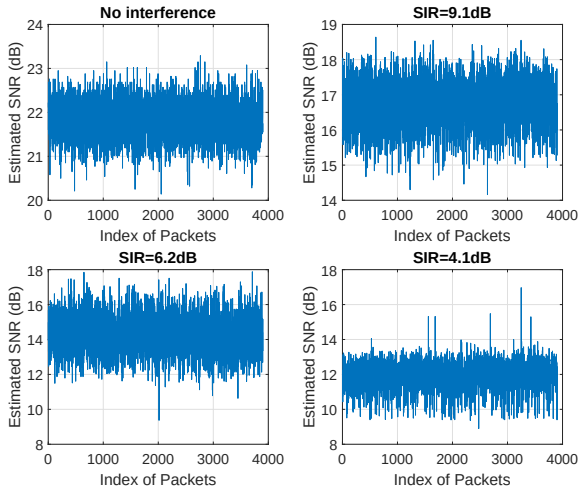

Fig. 10: Measured SNR values after interference suppression with different power levels of jamming signals.

have showcased the ability to sustain reliable communications in the presence of jamming signals in field conditions. Our separated lab trials, not presented here due to the page limit, demonstrated that the system worked well in the presence of even three jammers at different directions and locations to the receivers. This research paves the way for future advancements in tactical communication strategies, ensuring operational success in spectrum-warfare scenarios.

Acknowledgment

This research is supported by the Commonwealth of Australia as represented by the Defence Science and Technology Group of the Department of Defence.

References

[1] H. Pirayesh and H. Zeng, "Jamming attacks and anti-jamming strategies in wireless networks: A comprehensive survey," *IEEE Communications Surveys & Tutorials*, vol. 24, no. 2, pp. 767–809, 2022.

[2] Q. Yan, H. Zeng, T. Jiang, M. Li, W. Lou, and Y. T. Hou, "Jamming resilient communication using MIMO interference cancellation," *IEEE Transactions on Information Forensics and Security*, vol. 11, no. 7, pp. 1486–1499, 2016.

[3] H. Zeng, C. Cao, H. Li, and Q. Yan, "Enabling jamming-resistant communications in wireless MIMO networks," in *2017 IEEE Conference on Communications and Network Security (CNS)*, 2017, pp. 1–9.

[4] H. Pirayesh, P. K. Sangdeh, S. Zhang, Q. Yan, and H. Zeng, "Jamming-bird: Jamming-resilient communications for vehicular ad hoc networks," in *2021 18th Annual IEEE International Conference on Sensing, Communication, and Networking (SECON)*, 2021, pp. 1–9.

[5] H. Akhlaghpasand, E. Björnson, and S. M. Razavizadeh, "Jamming-robust uplink transmission for spatially correlated massive mimo systems," *IEEE Transactions on Communications*, vol. 68, no. 6, pp. 3495–3504, 2020.

[6] T. T. Do, E. Björnson, E. G. Larsson, and S. M. Razavizadeh, "Jamming-resistant receivers for the massive MIMO uplink," *IEEE Transactions on Information Forensics and Security*, vol. 13, no. 1, pp. 210–223, Jan 2018.

[7] A. Kekirigoda, K.-P. Hui, Q. Cheng, Z. Lin, J. A. Zhang, D. N. Nguyen, and X. Huang, "Massive mimo for tactical ad-hoc networks in rf contested environments," in *MILCOM 2019 - 2019 IEEE Military Communications Conference (MILCOM)*, 2019, pp. 658–663.

[8] Q. Cheng, Z. Lin, J. A. Zhang, D. Nguyen, X. Huang, A. Kekirigoda, and K.-P. Hui, "Multi-user mimo with jamming suppression for spectrum-efficient tactical communications," in *2020 14th International Conference on Signal Processing and Communication Systems (ICSPCS)*, 2020, pp. 1–6.